Broadening of spectral peaks at the merging of chaotic bands in period-doubling systems

Reggie Brown

Laboratory for Plasma and Fusion Energy Studies and Department of Physics and Astronomy,
University of Maryland, College Park, Maryland 20742

Celso Grebogi

Laboratory for Plasma and Fusion Energy Studies, University of Maryland, College Park, Maryland 20742

Edward Ott

Laboratory for Plasma and Fusion Energy Studies and Department of Physics and Astronomy,
and Department of Electrical Engineering, University of Maryland, College Park, Maryland 20742

(Received 27 February 1986)

For systems that undergo period-doubling cascades there also exists an "inverse cascade" of chaotic band mergings. The frequency spectrum associated with a chaotic orbit of 2^k constituent bands has 2^k δ-function spectral components superposed on a broadband continuous component. At merging, pairs of the 2^k bands join to produce 2^{k-1} bands. Associated with this, the number of δ-function spectral peaks halves. This happens via the acquisition of a finite spectral broadened width by every other δ function (hence making them no longer δ functions). This paper investigates this transition in detail with emphasis on its scaling properties.

I. INTRODUCTION

In many experiments in dissipative physical systems such as fluids, optical systems, plasmas, acoustics, solid state, etc., chaotic behavior is observed,[1] and changes in this behavior occur as some parameter is varied. Prominent among the characteristic changes in such systems is the period-doubling cascade. Here we shall be concerned with the effect of period-doubling cascades or power spectra of chaotic orbits. The power spectrum is usually the easiest, and often the only, quantity measured in a laboratory experiment. Therefore, the understanding of the properties of the power spectra is of fundamental importance for the correct intepretation of experimental results. Our numerical studies reported here are based on the one-dimensional quadratic map, $x_{n+1}=\mu-x_n^2\equiv F(x_n,\mu)$, where μ is a parameter. Although our results are for a particular F, universality[2,3] considerations imply that they should be general. As μ is decreased from a value at which chaotic motion takes place, a sequence of band splittings occur accumulating at $\mu_\infty=1.4011\ldots$. We define $\mu=\mu_k$ as the parameters value at which 2^{k-1} chaotic bands split into 2^k chaotic bands as the parameter μ is decreased (cf. Fig. 1 and caption).

If we take a point in one of these 2^k bands and iterate the map 2^k times, the point will come back to that band. However, if we examine the orbit every 2^k-th successive iterate, we see a chaotic-looking trajectory within the band. A discrete-time Fourier transform of the orbit reflects this situation; it consists of δ-function peaks at frequencies $\omega=n\omega_k$ [with $\omega_k\equiv2\pi(2^{-k})$ and $n=1,2,\ldots,2^k$] plus a continuum spectrum. (Recall that for discrete-time Fourier transform, ω lies between 0 and 2π.) The δ functions correspond to the fact that we know with absolute certainty that an orbit in a given band will

return precisely to that band 2^k iterates later; while the broadband continuum component of the spectrum reflects the chaotic motion within the bands. As μ increases from below μ_k to above μ_k the number of bands halves. Correspondingly, the number of δ functions must also halve. It is one of our purposes in this paper to investigate how the system accomplishes the transition from 2^k δ-function Fourier components to 2^{k-1} components. As we shall see, it does this by broadening each of the components at
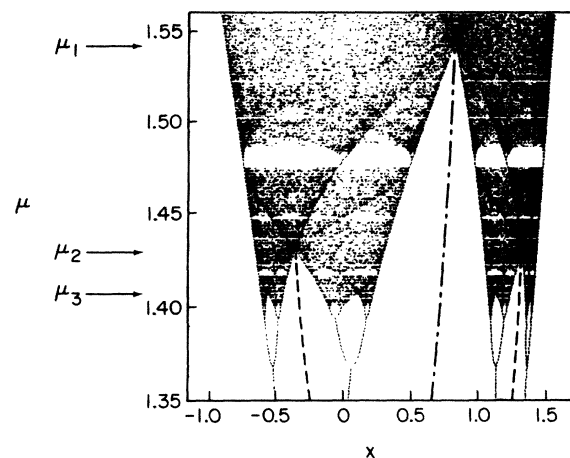

FIG. 1. Bifurcation diagram for the map $x_{n+1}=\mu-x_n^2$ in the range $1.35<\mu<1.56$. Within this range of μ values there is a countable infinity of band mergings. The mergings undergo an inverse cascade and accumulate at $\mu_\infty=1.4011\ldots$. We have labeled the first three consecutive band mergings by, respectively, μ_1, μ_2, and μ_3. The dashed-dotted line indicates an unstable period-1 orbit, while the dashed line indicates an unstable period-2 orbit.

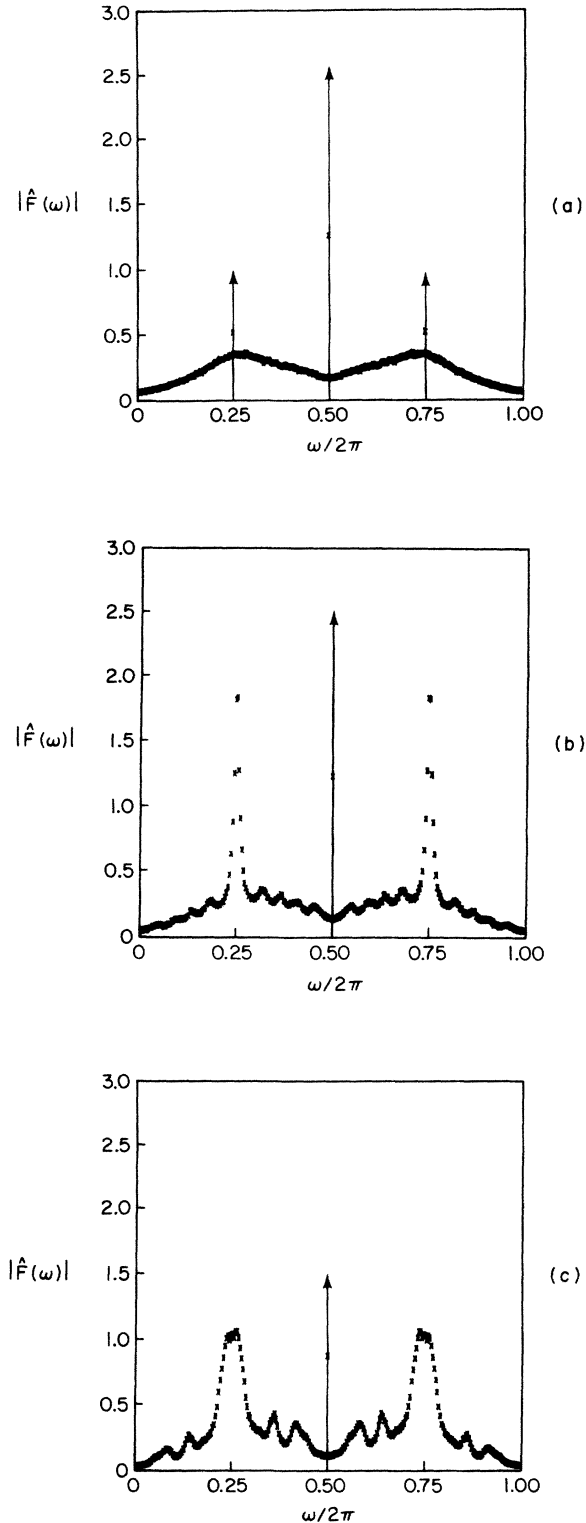FIG. 2. (a) Smoothed Fourier transform of an orbit x_n for $\mu=\mu_2=1.430\ldots$. Notice the δ function peaks at $\omega/2\pi=\frac{1}{4},\frac{1}{2}$, and $\frac{3}{4}$. (b) μ has been increased to $(\mu-\mu_1)/(\mu_1-\mu_2)$ $=0.0080\ldots$. Two of the peaks have broadened to a finite width, while the peak at $\frac{1}{2}$ is still a δ function. (c) μ has increased to $(\mu-\mu_1)/(\mu_1-\mu_2)=0.078\ldots$. The peaks continue to broaden and eventually become flat.

$\omega_k,3\omega_k,\ldots,(2^k-1)\omega_k$ into an approximately Lorentzian shape. The width of these Lorentzian components increases from zero as μ is raised from μ_k. As $(\mu-\mu_k)$ increases further the broadened peaks overlap and lose their individual identity. This is illustrated in Figs. 2 for $k=2$. Here we shall be mostly concerned with the scaling of the spectral widths for μ slightly greater than μ_k; that is, $\mu_{k-1}-\mu_k\gg\mu-\mu_k>0$. In addition, we shall also be interested in the $k\rightarrow\infty$ limit for which universal results apply. Previous work on the universal aspects of the power spectra of period-doubling cascades[4] has investigated the scaling of the strengths of the δ-function peaks, and the integrated noise power in the broadband feature.

Work related to the present paper has been done by Shenker and Kadanoff[5] who argue that the frequency-broadened width scales like $|\mu-\mu_k|^{-1/z}$ for a map of the form $F(x,\mu)=\mu-|x|^z$. The present paper considers only $z=2$ but reports more extensive analytical and computational results, and additional information not in Ref. 5; e.g., fine-structure deviations from the $|\mu-\mu_k|^{-1/2}$ dependence, computation of frequency spectra, and scaling as the accumulation of period doublings is approached.

In order to accomplish our goal we need to consider the process of band merging in more detail. In particular, consider the situation precisely at $\mu=\mu_k$. At the x values where the 2^{k-1} chaotic band splits to 2^k bands there is an unstable periodic orbit of period 2^{k-1} (e.g., in Fig. 1 the period-1 and the period-2 unstable orbits are labeled by the dashed-dotted and dashed lines, respectively). For $\mu_{k+1}<\mu<\mu_k$ the elements of the 2^{k-1} unstable orbit lie *outside* the bands and between them; for $\mu_{k-1}>\mu>\mu_k$ each of the 2^{k-1} bands *contains* an element of the unstable 2^{k-1} orbit. For $\mu_{k+1}<\mu<\mu_k$, a point in a given chaotic band is mapped under $F^{2^{k-1}}$ to the adjacent band with which it merges at $\mu=\mu_k$. In doing so, it necessarily crosses to the other side of that element of the unstable period 2^{k-1} orbit that lies between these two bands. For $\mu_{k-1}>\mu\geq\mu_k$, the elements of the unstable period 2^{k-1} orbit lie roughly in the centers of the 2^{k-1} chaotic bands, and we regard these elements as dividing each such band into two parts, which we call the left part (l) and the right part (r). Now consider a large number of iterates and examine a long succession of elements of the orbit that are 2^{k-1} iterates apart. Each of these lie in the same band, but may lie either in the left or right part of the band. Precisely at $\mu=\mu_k$ these 2^{k-1} separated iterates alternate from one side of the band to the other: $l,r,l,r,l,r,\ldots$. Above μ_k, l's, and r's do not necessarily alternate. Let $P_k(\mu)$ denote the fraction of times that the orbit fails to alternate from one part to the other; by "failing to alternate" we mean that an l is followed by an l or an r is followed by an r. [More precisely $P_k(\mu)$ is computed for a typical orbit in the limit that the length of the orbit goes to infinity.] Alternatively, we may think of $P_k(\mu)$ as the *probability* that an orbit does not cross from one side of the unstable element to the other side after 2^{k-1} iterates. [Clearly $P_k(\mu)\rightarrow0$ as $\mu\downarrow\mu_k$.] As we shall show, the probability of noncrossing events $P_k(\mu)$ determines the broadening of the spectral peaks at $\omega=\omega_k,3\omega_k,\ldots$. Thus we are led to a study of $P_k(\mu)$.

II. PROBABILITY OF NONCROSSING

To determine the behavior of $P_k(\mu)$, we performed extensive numerical experiments. A result of one such experiment is shown in Fig. 3 where in Fig. 3(a) the ordinate is the probability of noncrossing P_1 and the abscissa is the difference $\mu - \mu_1$ where $\mu_1 = 1.543 \ldots$ Figure 3(b) has the same information but is plotted in such a way as to make the systematic regularity in the results more apparent; namely, we plot $(\mu - \mu_1)^{1/2}/P_1(\mu)$ versus $\ln(\mu - \mu_1)$. We observe that (disregarding the small scale structure) P_1 appears to scale as $P_1 \sim (\mu - \mu_1)^{1/2}$.

In order to see how this scaling comes about consider the second iterate of the map:

$$x_{n+2} = \mu - (\mu - x_n^2)^2 \equiv F^2(x_n, \mu) \ .$$

Figure 4(a) shows the graph of this function for μ slightly less than μ_1 ($\mu_1 = 1.5436\ldots$). We observe that for this parameter value there are two disjoint chaotic regions R_A and R_B with the unstable fixed point $\tilde{x}_1 = 0.822\,87\ldots$ in between them. Under the first iteration $F(x,\mu)$ of the map, a point with, say, $x < \tilde{x}_1$ is mapped to $x' > \tilde{x}_1$, and, one iteration later, back to $x'' < \tilde{x}_1$. Thus, for $\mu < \mu_1$, the orbit remains on the same side of $\tilde{x}_1$ under the second iterate $F^2(x,\mu)$ of the map. Hence, the iteration of $F^2(x,\mu)$, as shown in Fig. 4(a), leaves R_A and R_B invariant.

However, for $\mu > \mu_1$ the situation is different, as shown by the graph in Fig. 4(b). Now, the regions R_A and R_B overlap with the unstable fixed point located in the overlap region $R_A \cap R_B$ and, as a result, R_A and R_B are no longer invariant under F^2. To determine the regions in R_A and R_B which do not cross $\tilde{x}_1$ under $F(x,\mu)$ we have to determine the regions in R_A and R_B which *do* cross to the other side of $\tilde{x}_1$ under $F^2(x,\mu)$. One of these regions is $R_1 \subset R_A$ centered at $x = 0$ which maps under $F^2(x,\mu)$ to $R_A \cap R_B$ and $x > \tilde{x}_1$, and the other region is $R_2 \subset R_B$ centered at $x = \mu^{1/2}$ which maps under $F^2(x,\mu)$ also to $R_A \cap R_B$ but to $x < \tilde{x}_1$. The range of R_1 (similar argument for the range of R_2) can be determined by noticing that one application of $F^2(x,\mu)$ sends any $x \in R_1$ into some $x < -\tilde{x}_1$. Another application of $F^2(x,\mu)$ then carried this point to $x > \tilde{x}_1$. Therefore, we are interested in all x such that $\mu - (\mu - x^2)^2 < -\tilde{x}_1$, or

$$|x| < [\mu - (\mu + \tilde{x}_1)^{1/2}]^{1/2} \equiv [G(\mu)]^{1/2} \ .$$

Since we are interested in $G(\mu)$ for μ near μ_1, we expand $G(\mu)$ in Taylor series about μ_1 to get

$$G(\mu) = G(\mu_1) + \Gamma_1^2(\mu - \mu_1) + \cdots \ , \tag{1}$$

where $\Gamma_1^2 \equiv \partial G / \partial \mu |_{\mu = \mu_1}$. By definition, $G(\mu_1) = 0$, and hence, $R_1 = \{x : \ |x| < \Gamma_1(\mu - \mu_1)^{1/2}\}$ and, by an analogous calculation, $R_2 = \{x : \ |x - \mu^{1/2}| < \Gamma_2(\mu - \mu_1)^{1/2}\}$, where Γ_2 is a constant. If the distribution of points in x generated by the orbit were smooth, then we would expect $P_1(\mu)$ to scale like the lengths of the interval R_1 and R_2; that is, $P_1(\mu) \sim (\mu - \mu_1)^{1/2}$. The distribution, however, is not smooth, in general, and thus we rewrite P_1 in the form
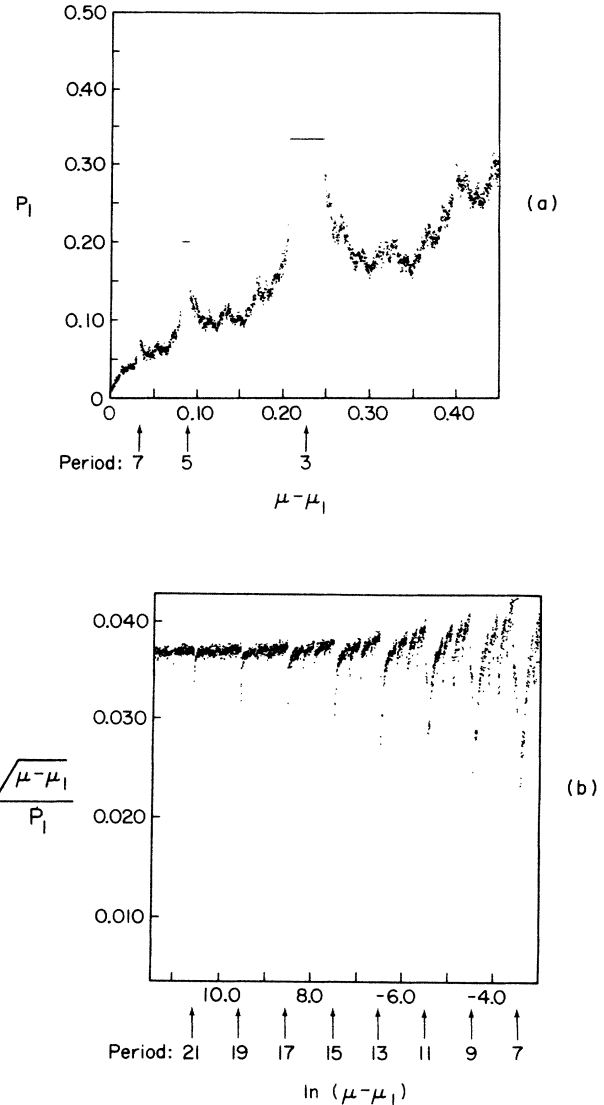

FIG. 3. (a) $P_1(\mu)$ vs $\mu - \mu_1$, where $\mu_1 = 1.543 \ldots$ We have indicated the periodic windows for periods 3, 5, and 7. (b) $(\mu - \mu_1)^{1/2}/P_1(\mu)$ vs $\ln(\mu - \mu_1)$. We have indicated the periodic windows for periods 7–21, inclusive.

$$P_1(\mu) = \frac{(\mu - \mu_1)^{1/2}}{W(\mu - \mu_1)} \ , \tag{2}$$

where the function $W(\mu - \mu_1)$ accounts for the lack of smoothness in the invariant distribution and leads to the fine-scaled detailed structure[6] that is seen in Fig. 3.

We have also examined $P_k(\mu)$ for $k = 2, 3, \ldots, 7$. We find that when $P_k(\mu)$ is expressed in terms of $\hat{\mu} = (\mu - \mu_k)/(\mu_{k-1} - \mu_k)$, it approaches a universal structure for large k. If we ignore the fine structure and examine the scaling of the upper envelope of $P_k(\mu)$ [e.g., see Fig. 3(b)], then we obtain

$$P_k(\mu)\simeq K\left[\frac{\mu-\mu_k}{\mu_{k-1}-\mu_k}\right]^{1/2}, \tag{3}$$

for $(\mu_{k-1}-\mu_k)\gg(\mu-\mu_k)>0$. Here the constant K is universal and numerically measured to be $K\simeq 21$.

III. FINE SCALE STRUCTURE OF $P_k(\mu)$

To understand the behavior of $W(\mu-\mu_1)$ we should realize that while the set of μ values yielding chaotic motion has positive measure, it is also believed that the intervals of μ yielding attracting periodic motion are dense.[7]
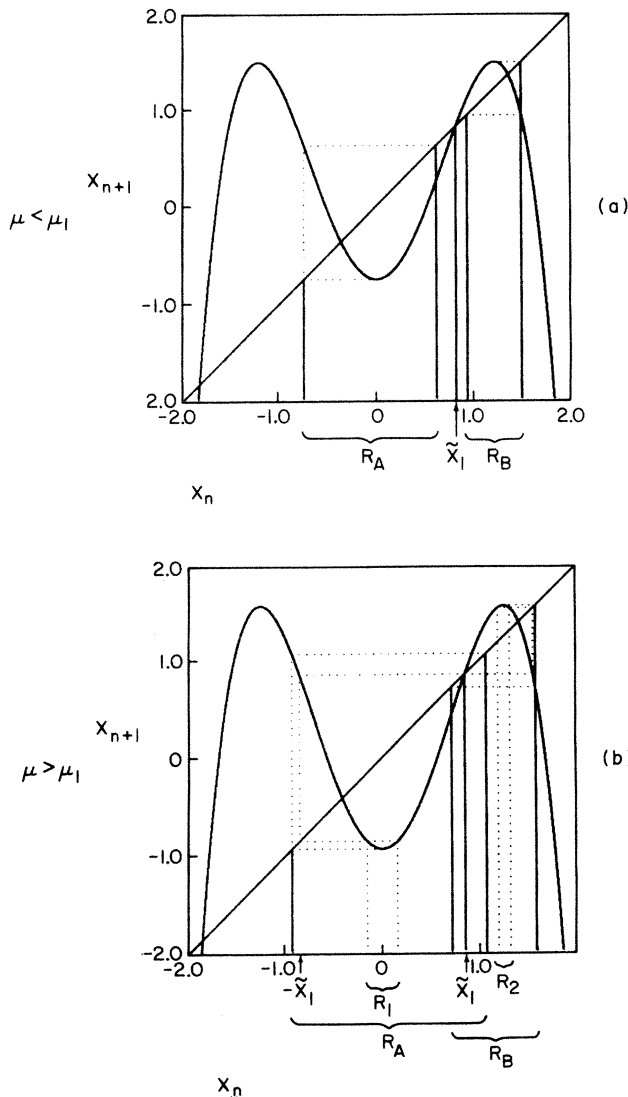
$\mu<\mu_1$

(a)

$\mu>\mu_1$

(b)

FIG. 4. (a) Graph of the function $x_{n+1}=F^2(x_n,\mu)$ for $\mu_1>\mu=1.5$. There are two invariant regions labeled R_A and R_B. A point that is mapped into one of these regions will remain in that region for all successive iterations. The unstable period-1 orbit lies between these two regions and is labeled $\tilde{x}_1$. (b) Now μ has been changed $\mu_1<\mu=1.587\ldots$. The regions R_A and R_B now overlap each other and are no longer invariant. The regions R_1 and R_2 are loss regions. A point that is mapped into $R_1\subset R_A$ will be mapped into R_B after two iterations of F^2. A similar statement applies to R_2.

The peaks with flat tops at $\mu-\mu_1\simeq 0.23$, 0.08, and 0.03 in Fig. 3(a) occur in the periodic windows of period 3, 5, and 7, respectively. They yield probabilities P_1 equal to $\frac{1}{3}$, $\frac{1}{5}$, and $\frac{1}{7}$, respectively. Since we have a dense set of μ intervals yielding attracting periodic orbits of different periods, we can expect P_1 to have a corresponding structure.

As an example, the Appendix presents an analysis for a particular family of windows. This particular family has odd period, $2N+1$, and it accumulates geometrically on μ_1 in the following way:

$$\mu(N)-\mu_1=c\delta^N, \tag{4}$$

where c and δ are constants given in the Appendix, and $\mu(N)$ denotes a characteristic value of μ in the stable range of the $2N+1$ period orbit [e.g., we can take $\mu(N)$ to correspond to the superstable condition for the $2N+1$ period orbit]. For μ in one of these period $2N+1$ windows, $P_1=1/(2N+1)$ and we obtain for W the result (cf. Appendix)

$$W(\mu(N)-\mu_1)\simeq\frac{2\ln[\mu(N)-\mu_1]}{\ln(\delta)}$$

$$\times\exp\{\tfrac{1}{2}\ln[\mu(N)-\mu_1]\}. \tag{5}$$

Figure 3(b) shows results of a numerical experiment involving 2^{12} orbits. We plot $(\mu-\mu_1)^{1/2}/P(\mu-\mu_1)\equiv W(\mu-\mu_1)$ versus $\ln(\mu-\mu_1)$. If we disregard the sharp dips due to the presence of periodic orbits, the graph is essentially constant, i.e., it indicates a constant value for $W(\mu-\mu_1)\simeq 0.037$ for chaotic orbits. The sharp downward dips correspond to orbits with μ values in the periodic windows. We indicate in Fig. 3(b) the periods of the major dips which correspond to the family of periodic orbits that led to Eqs. (4) and (5). From Eq. (4) we find that these dips are equally spaced in the logarithmic scale with a period given by $-\ln(\delta)$. We also note that the depth of these dips decreases exponentially as $\mu(N)\downarrow\mu_1$, as predicted by Eq. (5). For $N>3$ the tips of these dips cannot be discerned in Fig. 3(b) because their width decreases geometrically as $\mu(N)\downarrow\mu_1$ by the factor $7.9384\ldots$ (cf. Appendix). Our numerical computations confirmed this geometrical factor to 5 digits. In Fig. 3(b), we also observe that between the major dips there are smaller dips corresponding to other families of periodic orbits. In fact, as we have mentioned earlier, the μ values that yield periodic motion are thought to be dense. We can generalize our results, given in Eqs. (2) and (5), for $\mu=\mu_1$ to $\mu=\mu_k$, $k>1$, where we have to consider instead the map $x_{n+2}=F^{2^k}(x_n,\mu)$.

We have also performed numerical experiments near $\mu_2,\mu_3,\ldots,\mu_6$ and have found that the corresponding probabilities of noncrossing looks like that shown in Fig. 3(a) for μ_1 and appears to approach a universal structure for large k.

IV. POWER SPECTRA

Let $\{x_j\}_{j=0}^{j=M}$ be the trajectory of an initial point under the action of F. Then we define the Fourier transform of a function $G(x)$ for the sequence $\{x_j\}_{j=0}^{j=M}$ as

$$\hat{G}(\omega) = \frac{1}{\sqrt{M}} \sum_{j=0}^{M} G_j \exp(i\omega j) , \tag{6}$$

where $\omega = 2\pi l / M$, $l = 0,1,2,\ldots,M$, and $G_j \equiv G(x_j)$. The power spectrum is

$$\langle |\hat{G}(\omega)|^2 \rangle = \frac{1}{M} \sum_{j,k=0}^{M} \langle G_j G_k \rangle \exp[i\omega(j-k)] , \tag{7}$$

where the brackets $\langle \ \rangle$ indicate an ensemble average over initial conditions and $\langle G_j G_k \rangle \equiv C(j,k)$ is the autocorrelation function.

To determine $\langle |\hat{G}(\omega)|^2 \rangle$, as given by Eq. (7), we first calculate $C(j,k)$ for a specific convenient $G(x)$, as $\mu \downarrow \mu_1$ by defining a symbolic orbit in the following way: $x = -1$ for $x < \tilde{x}_1$ and $x = +1$ for $x > \tilde{x}_1$. That is, we consider the function $G(x) \equiv \mathrm{sgn}(x - \tilde{x}_1)$. We choose an initial condition with $x_0 < \tilde{x}_1$ and ask what is the probability that n iterates later the orbit has $x_n \leq \tilde{x}_1$, and what is the probability it has $x_n > \tilde{x}_1$. We assume that the orbit is in the chaotic region for which $P_1 \sim (\mu - \mu_1)^{1/2}$, and since $\mu - \mu_1 \ll 1$ we know that $P_1 \ll 1$. Furthermore, if we assume that the probability of a crossing at the nth iteration is determined solely by the probability at the $(n-1)$th iteration (i.e., there are negligible correlations[8]), then the average value of $\mathrm{sgn}(x - \tilde{x}_1)$ after n iterations is $(-1)^n(1 - 2P_1)^n \mathrm{sgn}(x_0 - \tilde{x}_1)$. Thus $C(j,k) = (-1)^{|j-k|}(1 - 2P_1)^{|j-k|}$, or

$$C(j,k) = (-1)^{j-k} \exp\{-|j-k| \ln[1/(1-2P_1)]\} . \tag{8}$$

Substituting Eq. (8) into Eq. (7) and taking $P_1 \ll 1$ into account, we obtain

$$\langle |\hat{G}(\omega)|^2 \rangle = \frac{1}{M} \sum_{j,k=0}^{M} \exp[i(j-k)(\omega-\pi) - 2|j-k|P_1]. \tag{9}$$

We now take the limit as $M \to \infty$ and perform the double sum to obtain

$$\langle |\hat{G}(\omega)|^2 \rangle = \frac{4P_1}{(\omega-\pi)^2 + 4P_1^2} - 1 . \tag{10}$$

Hence, we expect the expression for the power spectrum for a chaotic orbit, when $\mu \downarrow \mu_1$ to be a Lorentzian of the form given by Eq. (10) with a full width at half maximum given by $\Delta = 4P_1$. The result we just found for the Fourier transform of the function $G(x_n) = \mathrm{sgn}(x_n - \tilde{x}_1)$ (the "symbolic orbit") is also expected for other functions $G(x)$.

In our numerical experiments, done for the case $G(x) = x$, we choose a μ value and numerically find the power spectrum for an orbit of 2^{18} iterates. The spectrum is then smoothed to remove the noise from its structure. Figure 5 shows a typical smoothed power spectrum. The basic shape is that of a Lorentzian centered about $\omega/2\pi = \frac{1}{2}$, as it should be for $\mu \geq \mu_1$. A simplex algorithm is used to curve fit a Lorentzian to this peak and determine its width Δ. We repeat this procedure for 1800 values of μ, exponentially distributed as $\mu \downarrow \mu_1$ and plot $\Delta/(\mu-\mu_1)^{1/2}$ versus $\ln(\mu-\mu_1)$. The result is shown in Fig. 6. We notice that the fine scale structure is similar to
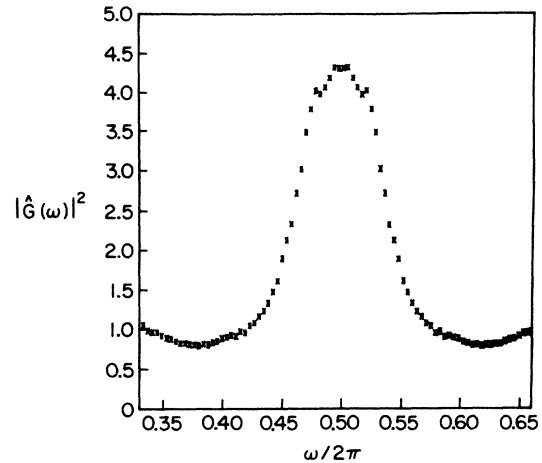

FIG. 5. Typical smoothed Fourier transform of an orbit x_n for $\mu > \mu_1$.

the one found in Fig. 3(b). We observe the same major dips with smaller dips in between. The periodicity exhibited by the major dips is $-\ln(\delta)$ as before. We can conclude then that the observed power spectrum can be understood from the probability of noncrossing.

V. CONCLUSION

In this paper we have discussed the scaling of the broadening of spectral peaks near values of the parameter at which band splittings occur. We find that the width Δ of peaks near $\mu = \mu_k$ scales roughly as

$$\Delta = 2P_k(\mu)\omega_k ,$$

where $\omega_k = 2\pi/2k$, and

$$P_k \simeq 21 \left[\frac{\mu - \mu_k}{\mu_{k-1} - \mu_k} \right]^{1/2}$$
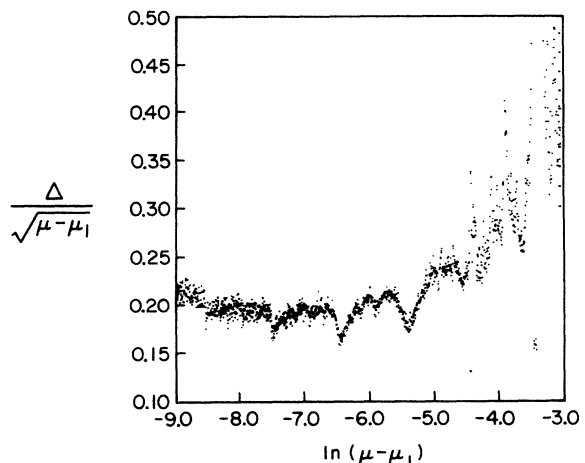

FIG. 6. Computer generated plot of $\Delta/(\mu-\mu_1)^{1/2}$ vs $\ln(\mu-\mu_1)$. Notice the similarity in structure to Fig. 3(b).

[cf. Eq. (3)]. Superposed upon this overall square-root dependence on $(\mu - \mu_k)$ we also find an intricate fine scale structure reflecting the occurrence of a dense set of periodic attractor windows. It appears likely that the overall square-root dependence of the broadening might be observed in experiments without excessive effort. The reliable experimental observation of the fine scale variations might be considerably more difficult, however.

ACKNOWLEDGMENTS

APPENDIX

In this Appendix we consider a particular family of periodic orbits. The family consists of primary orbits with odd period, $2N + 1$. The family is further characterized by having only one noncrossing. The probability of noncrossing, therefore, is $P_1 = 1/(2N + 1)$. Metropolis et al.[9] have studied the periodic orbits that arise in certain maps of the interval which have a single critical point ($F' = 0$ at a critical point). They consider superstable periodic orbits (i.e., orbits for which one of the elements is the critical point), and they characterize them by observing if the critical point was, under successive iterations of the map, mapped to the right or the left of the critical point. For our case, $F(x) = \mu - x^2$, and $x = 0$ is the critical point.

A point less than zero is labeled by an L, while a point greater than zero is labeled by an R. For example, for a superstable period-5 orbit say, the map iterates $x = 0$ as follows, $0 \to R \to L \to R \to R$, then we label this period-5 orbit RLR^2. For each superstable orbit of period M there is a range in μ about which this orbit is stable, and we call this a period M window. The family of windows we investigate here consists of those orbits whose superstable symbolic labels contain a single L which appears immediately after the first R and is followed by an unbroken string of R's.

We will define $\mu(N)$ as the μ value at which the $2N + 1$ orbit of our family is superstable. We will show that the distance in parameter space between $\mu(N)$ and μ_1 decreases geometrically,

$$[\mu(N) - \mu_1] \to c\delta^N , \qquad (A1)$$

as $N \to \infty$, with $c, \delta > 0$ and $\delta < 1$. We will also show that the width of the periodic windows also decreases geometrically, but at a faster rate.

For values of μ in the Nth periodic window of this family the probability of noncrossing is $P_1 = 1/(2N + 1)$. Solving Eq. (A1) for N we can rewrite the expression for the probability of noncrossing in the $2N + 1$ period window as

$$P_1 = \frac{\ln(\delta)}{2\ln[\mu(N) - \mu_1] - 2\ln(c) + \ln(\delta)}$$

$$\simeq \frac{\ln(\delta)}{2\ln[\mu(N) - \mu_1]} ,$$

where the second (approximate) equality applies for large N. Using this result and the definition of W and Eq. (2), we find

$$W(\mu(N) - \mu_1) \simeq \frac{2\ln[\mu(N) - \mu_1]}{\ln(\delta)} \exp\{ \tfrac{1}{2}\ln[\mu(N) - \mu_1]\} ,$$

which is Eq. (5).

Define $\Delta_N \equiv \mu(N) - \mu(N + 1)$. Thus (A1) gives

$$\Delta_N = [\mu(N) - \mu_1] - [\mu(N + 1) - \mu_1] \to c(1 - \delta)\delta^N ,$$

and $\Delta_{N+1}/\Delta_N \to \delta$ as $N \to \infty$. Thus if we can show that this ratio is true we will have proved the geometrical convergence.

From the definition of the mapping $x_{n+1} = F(x_n, \mu) \equiv \mu - x_n^2$, $\Delta_N = F(0, \mu(N)) - F(0, \mu(N + 1))$. After k iterations, the separation between iterates of $x = 0$ grows to

$$F^k(0, \mu(N)) - F^k(0, \mu(N + 1))$$

$$\simeq \Delta_N D_1(N) \cdots D_{k-1}(N) \equiv \widetilde{\Delta}(N, k) , \qquad (A2)$$

where

$$D_j(N) \equiv \frac{\partial F}{\partial x} \bigg|_{x = F^j(0, \mu(N))} .$$

For the Nth window, the sequence of R's and L's that characterize the orbit is RLR^{2N-2}. As such only $D_2(N)$ will be positive, while all the other $D_j(N)$'s will be negative. Since $1 \gg \Delta_N > 0$, $\widetilde{\Delta}(N, 2N + 1)$ will be negative and very small for large N.

At $\mu = \mu(N + 1)$, the origin will be mapped into itself after $2N + 3$ iterations. We can write this as

$$F^{2N+3}(0, \mu(N + 1)) = F^2(F^{2N+1}(0, \mu(N + 1)), \mu(N + 1))$$

$$= 0 .$$

If we insert Eq. (A2) into this expression we have

$$F^2(-\widetilde{\Delta}(N, 2N + 1), \mu(N + 1)) = 0 ,$$

where we have made use of $F^{2N+1}(0, \mu(N)) = 0$. We can solve this expression for $\widetilde{\Delta}(N, 2N + 1)$ to get

$$-\widetilde{\Delta}(N, 2N + 1) = \{\mu(N + 1) - [\mu(N + 1)]^{1/2}\}^{1/2} , \qquad (A3)$$

and similarly for the $(N + 1)$th window,

$$-\widetilde{\Delta}(N + 1, 2N + 3) = \{\mu(N + 2) - [\mu(N + 2)]^{1/2}\}^{1/2} . \qquad (A4)$$

Combining Eqs. (A3) and (A4), we obtain

$$\frac{\widetilde{\Delta}(N + 1, 2N + 3)}{\widetilde{\Delta}(N, 2N + 1)} = \left[\frac{\mu(N + 2) - [\mu(N + 2)]^{1/2}}{\mu(N + 1) - [\mu(N + 1)]^{1/2}} \right]^{1/2} . \qquad (A5)$$

In order to calculate Δ_{N+1}/Δ_N we must evaluate $D_j(N + 1)/D_j(N)$, for $j = 1, \ldots, 2N$. As an example, consider $D_1(N + 1)/D_1(N) = \mu(N + 1)/\mu(N)$, which we rewrite as $D_1(N + 1)/D_1(N) \equiv 1 - \Delta_N/\mu(N)$. In general, $D_j(N + 1)/D_j(N) = 1 + 0(\Delta_N)$. Hence, Eq. (A5) yields

$$\frac{\Delta_{N+1}}{\Delta_N} D_{2N+1}(N+1) D_{2N+2}(N+1)$$

$$\simeq \left[\frac{\mu(N+2)-[\mu(N+2)]^{1/2}}{\mu(N+1)-[\mu(N+1)]^{1/2}} \right]^{1/2} . \quad \text{(A6)}$$

The derivative $D_{2N+1}(N+1)$ and $D_{2N+2}(N+1)$ have to be evaluated to find a closed form expression for Δ_{N+1}/Δ_N. Recall that we defined $D_{2N+2}(N+1)$ as

$$D_{2N+2}(N+1) = \frac{\partial F}{\partial x} \bigg|_{F^{2N+2}(0,\mu(N+1))} .$$

Since $F^{2N+3}(0,\mu(N+1))=0$, we see that $F^{2N+2}(0,\mu(N+1))$ is just the preimage of the origin under F. Hence, $D_{2N+2}(N+1)=-2[\mu(N+1)]^{1/2}$, where we have used the positive square root because the last $2N$ iterates of the $(N+1)$th periodic windows are all positive. Similarly, $D_{2N+1}(N+1)=-2\{\mu(N+1) -[\mu(N+1)]^{1/2}\}^{1/2}$. Finally, if we insert the expression for $D_{2N+2}(N+1)$ and $D_{2N+1}(N+1)$ into Eq. (A6) we get

$$\frac{\Delta_{N+1}}{\Delta_N} = \frac{1}{4\mu(N+1)} \left[\frac{\mu(N+2)}{\mu(N+1)} \right]^{1/2}$$

$$\times \left[\frac{\left[1-\dfrac{1}{[\mu(N+2)]^{1/2}} \right]^{1/2}}{1-\dfrac{1}{[\mu(N+1)]^{1/2}}} \right]$$

$$\simeq \frac{1}{4\mu_1}(1-\mu_1^{-1/2})^{-1/2} \equiv \delta , \quad \text{(A7)}$$

where the last (approximate) equality comes about in the limit as $N \to \infty$. Equation (A7) can be put in the form of Eq. (A1). Thus we have proven Eq. (A1).

To graphically determine the value of δ, we consider a periodic window of period $2N+1$ and an adjacent window of period $2N+3$. From Eq. (A1) we have

$$\frac{\mu(N)-\mu_1}{\mu(N+1)-\mu_1} = \frac{1}{\delta} ,$$

or, by taking the logarithm of both sides

$$\ln[\mu(N)-\mu_1]-\ln[\mu(N+1)-\mu_1]=-\ln(\delta) .$$

Figure 3(b) has as its abscissa $\ln(\mu-\mu_1)$. The periodic windows are represented by downward pointing peaks. In this figure the quantity $-\ln(\delta)$ is the distance between adjacent windows. We observe that $-\ln(\delta)\simeq 1$ or $\delta^{-1}\simeq 2.7\ldots$, which is in agreement with the value predicted by Eq. (A7) of $\delta^{-1}=2.7277\ldots$.

Finally, we turn our attention to the convergence rate for the width of a periodic window. It is known that a periodic window in the chaotic regime of the quadratic map comes about via a saddle node bifurcation and ends in a crisis. Furthermore, it has been shown by Yorke et al.[10] that the width of a period $2N+1$ window scales like $\mu_c-\mu_0 \sim \lambda^{-4N}$, where μ_c and μ_0 are the parameter values at the crisis and saddle node bifurcation, respectively, and λ is the reduced Lyapunov[10] number of the map. By comparing the width of the Nth window with the width of the $(N+1)$th window we can determine λ. We have performed numerical experiments on the mapping $x_{n+1}=F(x_n,\mu)$ and have calculated $\mu_c-\mu_0$ for $N=1,2,\ldots,14$. From this data we have determined that

$$\frac{\mu_c(N)-\mu_0(N)}{\mu_c(N+1)-\mu_0(N+1)}=\lambda^4=7.9384\ldots .$$

Thus we have shown that both the width of the windows and the distance between them converge geometrically to zero as $N\to\infty$. The width converges at a rate $\lambda^4=7.9384\ldots$, while the distance between them converges at the slower rate of $\delta=2.7277\ldots$.

[1]See, for instance, E. Ott, Rev. Mod. Phys. 53, 655 (1985), and references therein.

[2]M. J. Feigenbaum, Physica D 7, 16 (1983).

[3]J.-P. Collet and J.-P. Eckmann, Iterated Maps of the Interval (Birkhauser, Boston, 1980).

[4]M. J. Feigenbaum, Phys. Lett. 74A, 375 (1979); M. Nauenberg and J. Rudnick, Phys. Rev. B 24, 493 (1981); B. A. Huberman and A. B. Zisook, Phys. Rev. Lett. 46, 626 (1981); A. Wolf and J. Swift, Phys. Lett. 83A, 184 (1981); S. Thomae and S. Grossman, ibid. 83A, 181 (1981).

[5]S. J. Shenker and L. P. Kadanoff, J. Phys. A 14, L23 (1980). (We became aware of this work after completion of our present paper.)

[6]For similar considerations see the discussion of Fig. 5 of the paper by C. Grebogi, E. Ott, and J. A. Yorke, Physica D 7, 181 (1983).

[7]M. V. Jakobsen, Commun. Math. Phys. 81, 39 (1981).

[8]The neglecting of such correlations is a good approximation for $\mu\downarrow\mu_1$ since then the orbit length between crossings is long ($P_1 \ll 1$), and the motion is chaotic.

[9]N. Metropolis, M. L. Stein, and P. R. Stein, J. Comb. Theory Ser. A 15, 25 (1973).

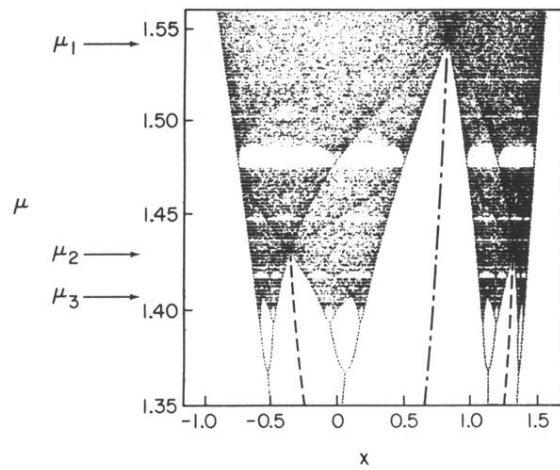[10]J. A. Yorke, C. Grebogi, E. Ott, and L. Tedeschini-Lalli, Phys. Rev. Lett. 54, 1095 (1985).

FIG. 1. Bifurcation diagram for the map $x_{n+1} = \mu - x_n^2$ in the range $1.35 < \mu < 1.56$. Within this range of μ values there is a countable infinity of band mergings. The mergings undergo an inverse cascade and accumulate at $\mu_\infty = 1.4011 \ldots$. We have labeled the first three consecutive band mergings by, respectively, μ_1, μ_2, and μ_3. The dashed-dotted line indicates an unstable period-1 orbit, while the dashed line indicates an unstable period-2 orbit.